Solar-Array-Induced Disturbance of the Hubble Space Telescope Pointing System

C. L. Foster, M. L. Tinker, G. S. Nurre, W. A. Till

Reprinted from

Journal of Spacecraft and Rockets

Volume 32, Number 4, Pages 634–644

AIAA

A publication of the
American Institute of Aeronautics and Astronautics, Inc.
370 L'Enfant Promenade, SW
Washington, DC 20024-2518

JOURNAL OF SPACECRAFT AND ROCKETS
Vol. 32, No. 4, July–August 1995

Solar-Array-Induced Disturbance of the Hubble Space Telescope Pointing System

Carlton L. Foster,* Michael L. Tinker,† Gerald S. Nurre,‡ and William A. Till§
NASA Marshall Space Flight Center, Huntsville, Alabama 35812

The investigation of the vibrational disturbances of the Hubble Space Telescope that were discovered soon after deployment in orbit is described in detail. It was found that the disturbances were particularly evident during orbital day–night crossings, and that the magnitude of the disturbances was considerably larger than the design jitter requirement. This paper describes the process by which the vibrations were characterized and isolated to a particular mechanism. The analysis of the flight data and comparisons with computer simulation results showed that the source of the disturbances was the thermally driven deformation of the solar arrays in conjunction with frictional effects in the array mechanisms. The control system was successfully modified to attenuate the disturbances to tolerable levels pending mechanical and thermal redesign of the solar arrays. The new arrays were installed during the first Space Telescope servicing mission, and in combination with the enhanced control system algorithm reduced the disturbances to satisfactory levels.

Nomenclature

$[F]$	= external force vector, lb
$[F(t)]$	= vector of solar-array tip forces, lb
$[I]$	= identity matrix
$[K]$	= stiffness matrix, lb/in.
$[M]$	= mass matrix, lb · s^2/in.
$\{q\}$	= generalized displacement
$[R]$	= rigid-body transformation matrix
$[T_1]$, $[T_2]$	= displacement transformation matrices
$\{x\}$	= displacement, in.
$[\zeta]$	= matrix of damping ratios
$[\Phi]$	= mode shape matrix
$[\omega^2]$	= matrix of natural frequencies squared, s^{-2}

Subscripts and Superscripts

b	= boundary degrees of freedom
c.g.	= center of gravity
q	= generalized degrees of freedom
sa	= solar arrays
sys	= coupled telescope system
*	= free-boundary and transformed modes

Introduction

THE Hubble Space Telescope (HST)[1] was deployed from the remote manipulator system of the Space Shuttle Discovery in a 332-n mile orbit on April 25, 1990. Within several orbits it became clear from observing real-time telemetry data that the pointing control system was experiencing unexpectedly large disturbances that were most pronounced as the spacecraft entered or left Earth's shadow. A concerted investigative analysis during the following weeks pointed to the solar arrays as the source of the disturbance. The thermal and mechanical energy in the arrays was stored and released in such a manner as to excite the primary modes of the arrays and thus perturb the pointing control system. The HST is shown in Fig. 1 and is normally operated so that the sun is in the V1–V3 plane, confined to the angles shown. The solar arrays are oriented about V2 to point in the direction of the sun. The European Space Agency and British Aerospace provided the solar arrays. The design is based on that of the flexible rolled-up solar array described in Ref. 2. The other major parts of the HST are the optical telescope assembly made by Hughes Danbury Optical Systems and the support systems module built by Lockheed Missiles and Space Company.

The paper begins with a section describing the solar arrays and their mechanisms, providing information that is essential to understanding the disturbance phenomena. Next is a section that shows and describes some of the flight data that illustrate the characteristics of the disturbance as it affected the pointing control system. Following these introductory topics, the analysis of the disturbance and the explanation of the phenomena are presented.

Description of Original Solar-Array Mechanisms

The HST solar arrays consist of two identical wings. Each wing has two flexible solar-cell blankets attached to a drum, which rotates about a central spar tube or boom. The drum and spar tube are parts of the secondary deployment mechanism, which was designed to provide structural support of the solar arrays during launch and to deploy the blankets on orbit. For launch, the two blankets and an embossed cushion were rolled tightly about the drum and locked in position. The boom was secured to the forward shell and light shield of the HST by means of structural latches. On orbit, the latches were released and the booms pivoted 90 deg by the primary deployment mechanism. The secondary deployment mechanisms then deployed the blankets from the drums via spreader bars attached to a pair of BI-STEM booms. As the blankets were deployed, the cushion was taken up on a storage roller. The overall Space Telescope configuration is shown in Fig. 1, and the solar-array deployment is illustrated in Fig. 2. Reference 3 gives a detailed description of the secondary deployment mechanism design and development.

The BI-STEM (two-element storable tubular extendable member) is made from thin strips of stainless steel formed into circular cross sections that were flattened and stored on spools or cassettes within the mechanism. The elements were rolled from the spools through specially shaped guides and nested together with the open seams diametrically opposed, forming the tubular structure of the boom. Two booms were deployed in opposite directions from the actuator assembly as shown in Fig. 3. The secondary deployment mechanism assembly includes both inboard and outboard actuators, mounted on the main spar on either side of the drum. The actuator assemblies are connected via a torque tube, so that all four booms were driven by a motor located in the outboard end of the spar. The actuator

Received Oct. 29, 1993; revision received Jan. 9, 1995; accepted for publication Jan. 20, 1995.

*Support Equipment Branch, Mechanical Systems Division.
†Dynamics and Loads Branch, Structural Analysis Division. Member AIAA.
‡Chief Scientist, Pointing Control Systems, Structures and Dynamics Laboratory.
§Systems Thermal Design Branch, Thermal and Life Support Division.

assembly includes limit switches on each boom that sensed a fully deployed or retracted condition; any switch was capable of cutting off the drive motor when the limit to travel was reached. Figure 4 shows the actuator mechanism.

The spreader bars were attached to rails mounted at the tips of the BI-STEMs through a system of steel tapes, rollers, tension springs, and linear potentiometers, which constituted the boom length compensation mechanism. This system, along with a pair of negator springs that drove the drum, provided the blanket tension. It also compensated for small length differences among the four booms, which could have occurred during deployment or retraction because of friction effects at the guides or within the multiple layers of the rolled-up elements stored on the cassettes. The original boom length compensation mechanism is illustrated in Fig. 5.

The drum rotates on the central spar tube on dry-lubricated ball bearings mounted in end supports. The outboard bearing is free to slide axially to accommodate differential expansion between the drum and the tube. The end support also includes a diaphragm section to limit bearing axial loading should the sliding interface fail. For the original arrays, thermal expansion and contraction of the blankets and booms were accommodated by small-angle rotations of the drum. Blanket tension was maintained by the constant-torque negator springs.

During deployment, the spreader bars moved out along the compensator rails following the drum lock release to a position where the tension of the linear springs in the compensation mechanisms balanced the negator spring tension. If the booms were not synchronized during deployment, the linear potentiometer and spring should have moved within the spreader bar as the attachment bracket roller moved backward along the rail of the leading boom and the opposite roller moved forward on the lagging boom. This action was designed to keep the spreader bar parallel to the drum throughout the deployment, in order to maintain constant blanket tension. The four booms should have extended until the limit switch of one boom was reached and the motor was cut off. During ground testing of the secondary deployment mechanism, overall boom synchronization was within approximately 1 in. total among the four booms at the fully deployed position. After the motor stopped, the spreader bars should have remained in equilibrium position on the rails.

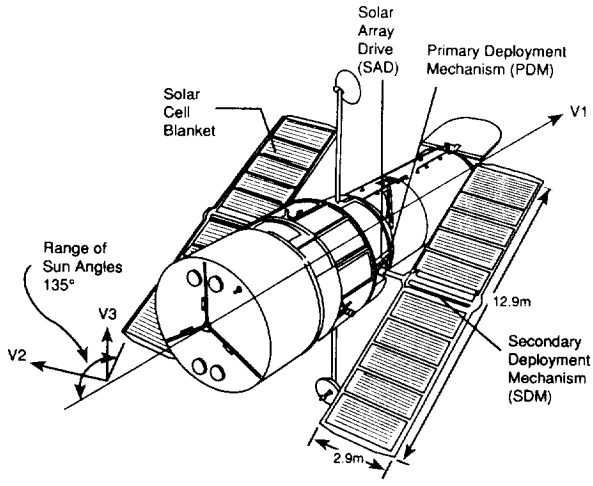

Fig. 1 Hubble Space Telescope on-orbit configuration.

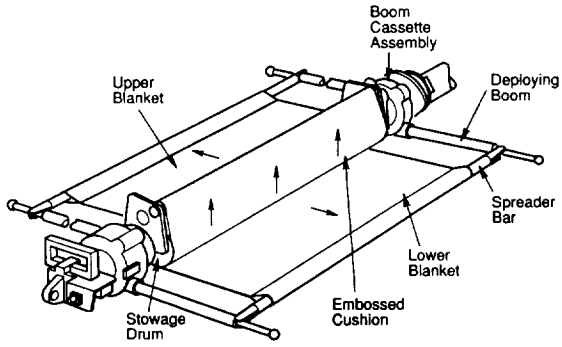

Fig. 2 Solar-cell blanket deployment.

On-Orbit Deployment Sequence Anomalies

The solar arrays were successfully deployed with the HST positioned above the orbiter cabin and held by the remote manipulator system. There were a few minor anomalies encountered during the deployment sequence, which resulted in delays to the nominal timeline. The removal of the HST from the orbiter cargo bay and its positioning in the appendage deployment attitude using the remote manipulator system were completed without incident, but required approximately 30 min longer than expected. Completion of primary deployment system operations was also delayed by several minutes because of an anomaly in the position-switch adjustments. A contingency procedure had to be implemented to verify the final position of the solar-array masts. The mechanisms had functioned correctly, but the telemetry was ambiguous. As a result of these delays, subsequent appendage deployment events had to be replanned in order to comply with the constraints on minimum time in sunlight, time remaining in sunlight, and windows of uninterrupted communication.

The secondary deployment mechanism (SDM) operation for the +V2 solar array was completed with no anomalies. However, the −V2 SDM motor cur off immediately after the drum lock was released, and telemetry indicated a blanket tension test failure. The SDM commands were sent again, and the blankets deployed

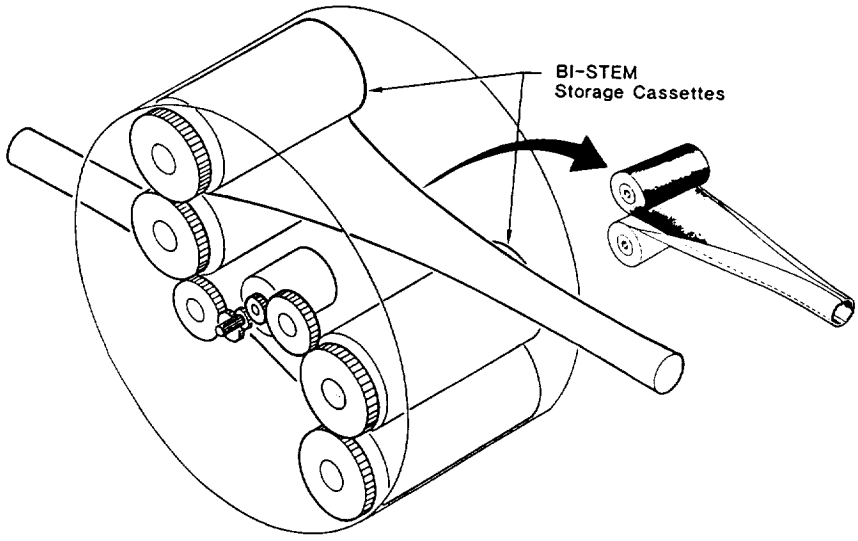

Fig. 3 Solar-array boom actuator drive train.

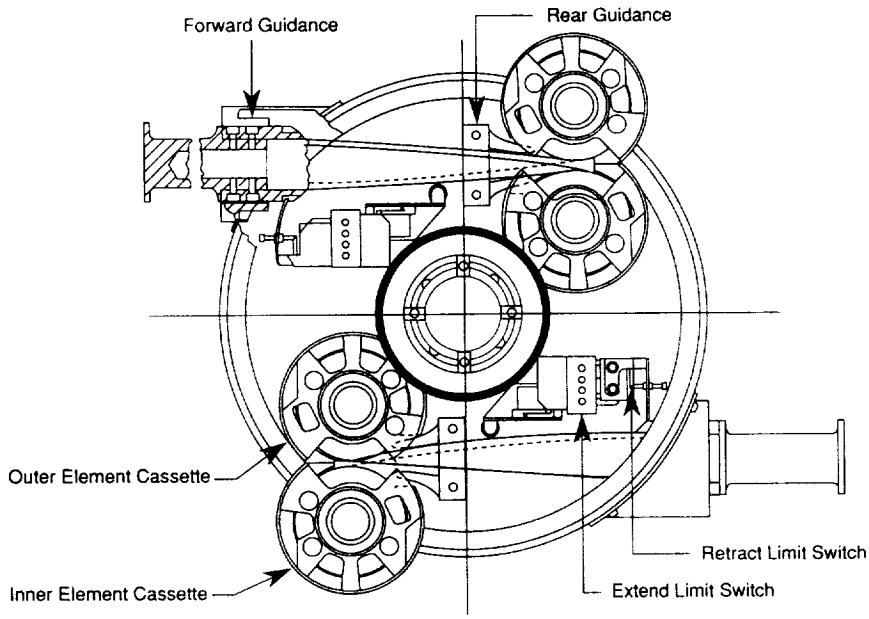

Fig. 4 Boom actuator mechanism.

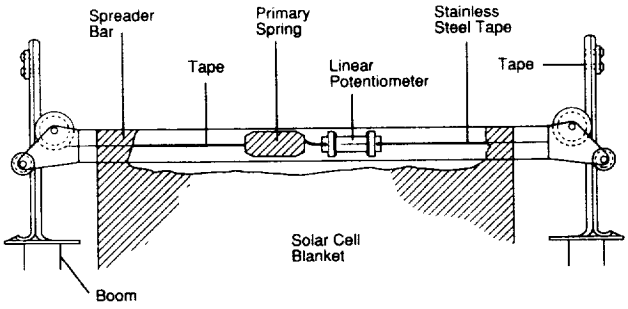

Fig. 5 Boom length compensation mechanism for original solar arrays.

Fig. 6 Hubble Space Telescope shortly after release from Shuttle Orbiter.

approximately 1.5 m before the motor was cut off again by the blanket tension test. A visual check of the spreader-bar position on the compensator rails verified that the blanket tension was nominal. It was decided to bypass the blanket tension test, and the −V2 deployment was completed successfully on the third try. Later, a failure investigation showed that the tension test had shut down the SDM because of an intermittent open circuit in the −V2 upper blanket tension potentiometer. This potentiometer continued to give erratic readings, with changes in the signal corresponding to the sunlit and eclipse periods of each orbit. Because there was no corresponding change to the tension reading of the other blanket on the −V2 solar array, it is possible that the problem was simply an electrical fault, unrelated to the disturbance phenomenon.

Photographs taken after release of the HST (Fig. 6) indicate that the inboard boom of the upper blanket on the −V2 array had a significant curvature, which resulted in a twist at the spreader bar of as much as 12 deg out of the plane of the blankets. Possible relevance of this twisting to the vehicle disturbance phenomenon is discussed in a later section.

Manifestation of the Disturbance

The pointing control system was designed to hold an image stable at the HST focal plane to 0.007 arcsec (rms) for the duration of an observation, which varies from a few seconds to a few hours. Consequently, careful attention was given to restricting the magnitude of internal disturbances and to carefully characterizing those disturbances that appeared to be most threatening to observations. In the case of the solar arrays, a disturbance level was specified for steady-state operation that is consistent with the pointing requirements, and care was taken in designing HST and solar-array maneuver profiles to minimize the excitation of the solar-array modes. Hence, the phenomenon giving rise to the data in Figs. 7 and 8 was indeed a surprise. The two figures together show attitude excursions of the line of sight of the HST for the day and night portions of two noncontiguous orbits. The orientation of the solar arrays during these times was such that the plane of the array was in the V2–V3 plane.

The attitude data were derived from the rate gyro signals onboard the HST. The gyro data, available every second, were integrated and resolved into the principal spacecraft coordinates. Angular motions about V2 and V3 define the line of sight of the telescope, and angular motion about V1 is roll about the line of sight. Figure 7 shows the attitude time history for the three axes for the daylight portion of an orbit beginning with the transition from earth's shadow (eclipse) to orbital day. The effects of the disturbance associated with the transition are clearly evident with amplitudes in V2 and V3 of approximately 0.1 arcsec. Later data showed disturbance amplitudes about V3 of 0.2 arcsec. The transition event lasted 4–5 min. Following the night–day transition there was a series of disturbances that persisted through most of the orbital day and that had amplitudes nearly as large as those at the terminator. Then, toward the end of the day, the disturbances waned, and a quiet period was seen for 8–10 min prior to entry into the Earth's shadow at 22.65 h. The transition to darkness gave rise to another large attitude disturbance, which showed larger amplitudes than the night–day transition. Figure 8 shows the night portion of an earlier orbit. The first 14 min again showed a quiet period just prior to entry into darkness at 11.34 h. At

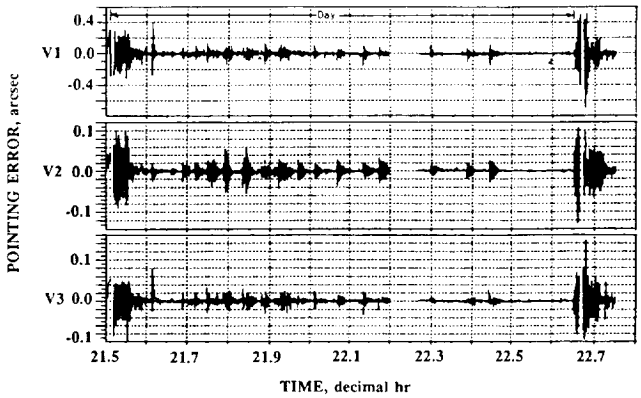

Fig. 7 Orbital day disturbance profile.

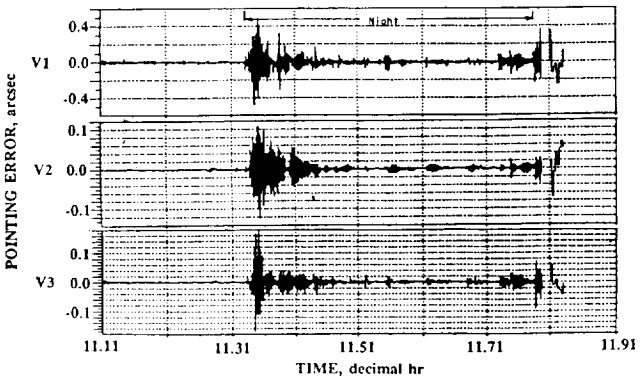

Fig. 8 Orbital night disturbance profile.

the day-to-night transition a large disturbance occurred, with amplitudes in V2 and V3 in excess of 0.1 arcsec. The transition event lasted 3–4 min and was followed by a series of separate disturbances that persisted through the night.

These attitude time histories are representative of the dynamic behavior of the HST as it was seen from orbit to orbit. In general, the transition disturbances were largest, the disturbances subsided completely during the latter part of the day, and the night was quieter than the early day. The pointing disruptions associated with these disturbances were of sufficient magnitude to compromise many of the science goals of the HST.

Disturbance Identification and Characterization

Investigation of the HST vibration problem was twofold. First, the source of the vehicle disturbance was identified. This was accomplished by comparison of the characteristics of possible excitation sources with the on-orbit telemetry data describing the disturbances. Next, dynamic mathematical models of the telescope were assembled or developed in attempts to analytically characterize the disturbances and their effects on the vehicle motion. In the following sections the process of isolating the source of the transitional and orbital day disturbances and the procedure of analytically modeling the transitional disturbances are described. Results of mathematical models are used to verify the identification of the disturbances.

Further Description of Vehicle Disturbances

Detailed examination of the telemetry data (Fig. 9) for the rate gyro assembly revealed a beating phenomenon, particularly for rate gyro 5. This beating provided an early indication that either two disturbances with closely spaced frequencies were exciting the telescope or the source of excitation was affecting two closely spaced modes of the structure. These oscillations were estimated to be 2 to 3 orders of magnitude greater than the allowable jitter for the telescope, obviously large enough to prevent focusing on distant objects. The data shown in Fig. 9 corresponded to an orbital day-to-night transition, and were obtained from Ref. 4.

Also in Fig. 9, the frequency spectra corresponding to the disturbances time histories are shown. Although these spectra represent a single average of raw telemetry data without windowing or bias removal, the dominant frequencies can be observed. It is seen that the disturbance occurred at approximately 0.1 Hz. Rate gyro 5 showed a second large frequency component near 0.12 Hz, verifying the beating phenomena shown in the time history data. These frequency components of the disturbance occurring during transition to eclipse were also obtained in an independent data analysis as described in Ref. 5. For convenience in the analysis, the vehicle rotations were transformed to the (V1, V2, V3) axes of the telescope (Fig. 1). The vehicle rates about these axes for one sunlight–eclipse transition are shown in Fig. 10 to illustrate the onset of disturbance at the time of transition and the subsequent damping of the oscillations. Analysis of the frequency content of the (V1, V2, V3) oscillations showed dominant frequencies of approximately 0.1 Hz for the V1 and V2 axes and 0.6 Hz for the V3 axis. The 0.1-Hz component was also well defined for the V3 axis.

Disturbances occurring during the orbital days and eclipse–sunlight transitions were observed to have considerably different characteristics than the sunlight–eclipse disturbances. In Fig. 11, the vehicle rates about the (V1, V2, V3) axes are shown for one eclipse–sunlight transition and the following period of approximately 18 min. The initial disturbance occurring near decimal hour 13.63 was followed by a quiet period of about 6 min, and then another series of oscillations of slightly lower amplitude than the initial disturbance. At the left of Fig. 11 is a large spike corresponding to a vehicle maneuver. Oscillations occurring during the quiescent orbital day (well past the eclipse-to-sunlight transition) are shown in Fig. 12. These disturbances exhibited damping and a well-defined decay pattern; the beating behavior was less prominent than for the transitional vibrations. The smooth decay of the oscillations in Fig. 12 could indicate that one excitation source was primarily responsible for the quiescent day disturbances. For both types of disturbances discussed in this paragraph, prominent frequencies were again 0.1 Hz for the V1 and V2 axes and 0.6 Hz for the V3 axis.

Determination of Disturbance Source

Several potential sources of the HST disturbances were identified in Ref. 5 and by other investigators. These mechanisms included the reaction-wheel assemblies, data recorders, fine guidance sensors, high-gain antennas, aperture door, magnetic torquers, support systems module (thermal creak), pointing control system, and solar arrays. All of the potential sources were investigated systematically in view of the telemetry data, which showed that the disturbances occurred mainly near 0.1 Hz.

The reaction-wheel assemblies, data recorders, and fine guidance sensors all operate at very low force and moment levels (millipounds and milli-inch-pounds) and frequencies considerably higher than 0.1 Hz. The reaction-wheel assemblies have one harmonic at 0.35 Hz, but the jitter test of the telescope showed that this harmonic does not significantly excite the vehicle. The major response of the data recorders occurs at 1.4 Hz at very low disturbance levels, and the fine guidance sensors have no output below 1 Hz. In addition, the vehicle disturbances were observed whether or not the fine guidance sensors were in operation. Based on these findings, it was concluded that none of the three mechanisms discussed in this paragraph could have caused the disturbances.

Boom bending modes of the high-gain antennas occur between 0.4 and 1.0 Hz and can only be excited when the telescope is oriented with the −V1 axis into the sun (Fig. 1). In addition, there was no correlation between the disturbances and movement of the antenna gimbals. The aperture door and magnetic torquers both have consistent responses during both transient and nominal conditions. Therefore, none of these mechanisms could have contributed unusual excitations during the disturbances.

Thermal creak is a phenomenon where energy built up in tight joints due to thermal expansion or contraction is suddenly released as friction force.[5] This phenomenon has a broadband frequency spectrum, with most of the energy occurring in the high-frequency region (50–100 Hz). For thermal creak in the support systems module to excite a 0.1-Hz oscillation, it should have also excited

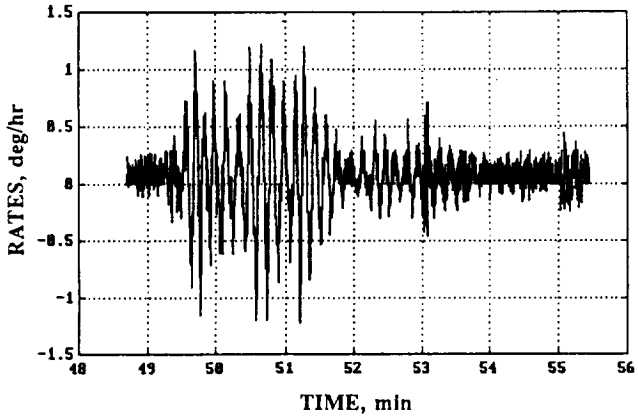

a) Rate gyro 4

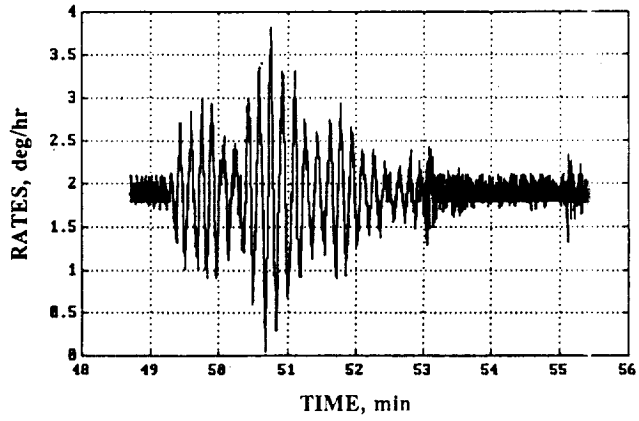

c) Rate gyro 5

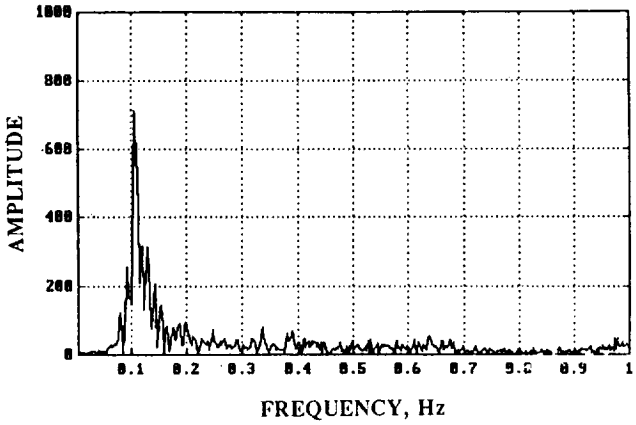

b) Rate gyro 4

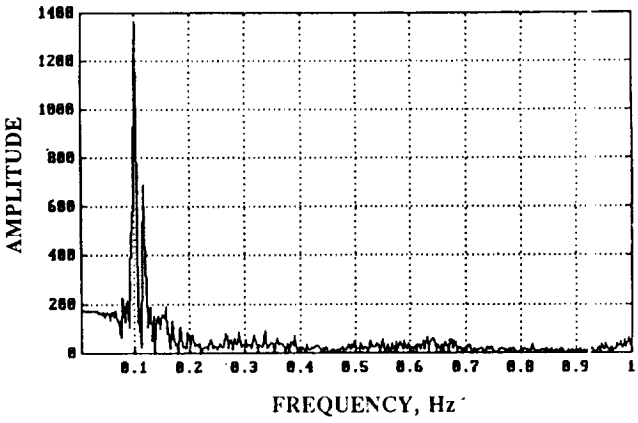

d) Rate gyro 5

Fig. 9 Rate gyroscope disturbance data: a) gyro 4 time history, b) gyro 4 frequency spectrum, c) gyro 5 time history, and d) gyro 5 frequency spectrum.

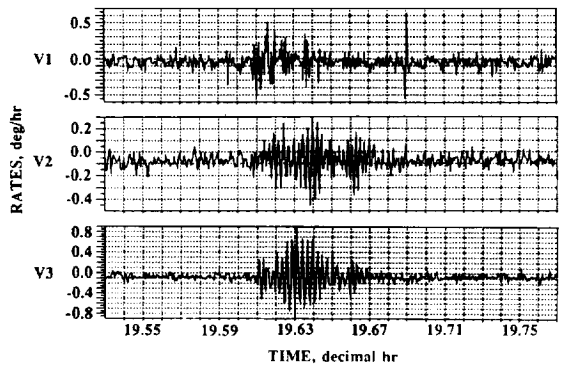

Fig. 10 Rate disturbances about (V1, V2, V3) axes for sunlight–eclipse transition.

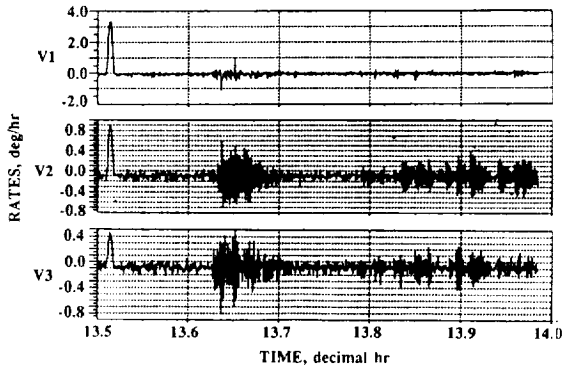

Fig. 11 Vehicle disturbances about (V1, V2, V3) axes for eclipse–sunlight transition.

all the low-frequency modes of the module. Since this was not observed in the telemetry data, it was concluded that thermal creak in the support systems module did not cause the vehicle disturbances.

Two remaining mechanisms were considered as possible sources of the vehicle rate disturbances: the pointing control system and the solar arrays. Since the control system actively alters the vehicle rotation rates throughout the orbit,[5] it was thought that the controller could cause the oscillations. However, the time histories in Fig. 13 for the vehicle rates and the total system torque show that the control torques always oppose and lag behind the vehicle rates. Therefore, the control system could not have induced the disturbances.[6] However, since the controller had a minimum in its gain margin[5] at about 0.1 Hz, it appears that the control system in its nominal configuration was unable to damp the vehicle disturbances adequately.

By the systematic investigation and process of elimination described in this section, it was concluded that the solar arrays were the source of the vehicle rate disturbances. The evidence supporting this conclusion was strong: 1) the fundamental bending modes of the arrays were predicted[7] to be near 0.1 Hz (Fig. 14), 2) the beating phenomena observed in the oscillation time histories could be explained in terms of slight stiffness variations between the two arrays, and 3) the highly flexible arrays were the most logical sources of disturbance for the orbital transitions where large thermal gradients were built up between the hot and cool surfaces of the spacecraft. In addition, the observed rotations of the vehicle changed in direct correlation with changes in solar-array orientation.[5]

To identify possible mechanisms of the solar arrays causing the disturbances, it was first necessary to determine the thermal characteristics of the arrays. It was recognized that the steel deploying

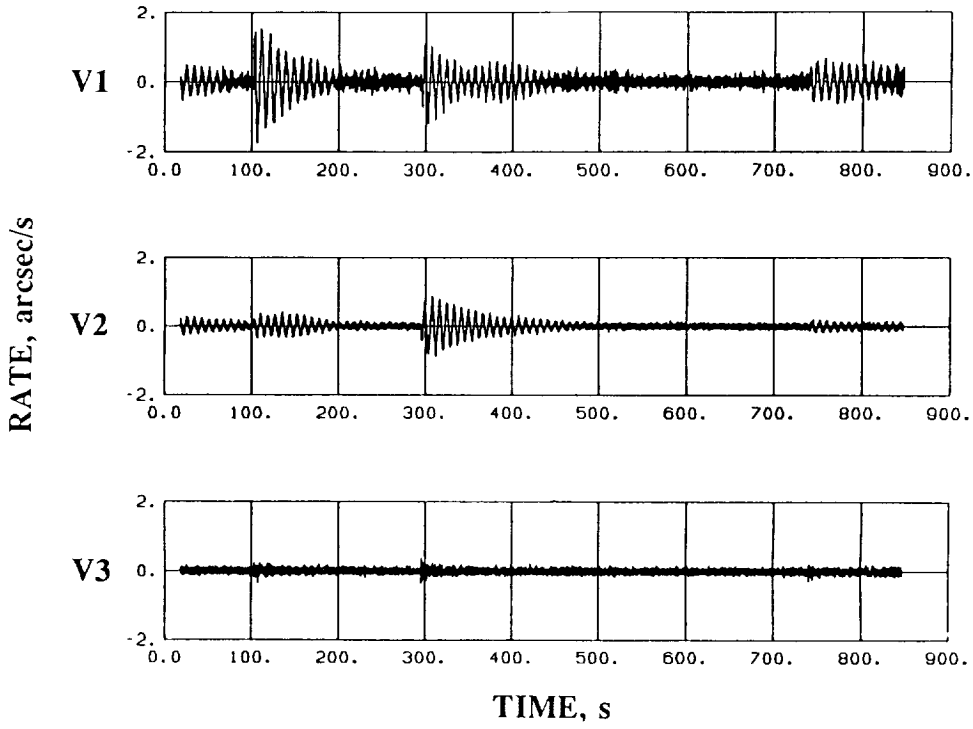

Fig. 12 Orbital day vehicle rate disturbances.

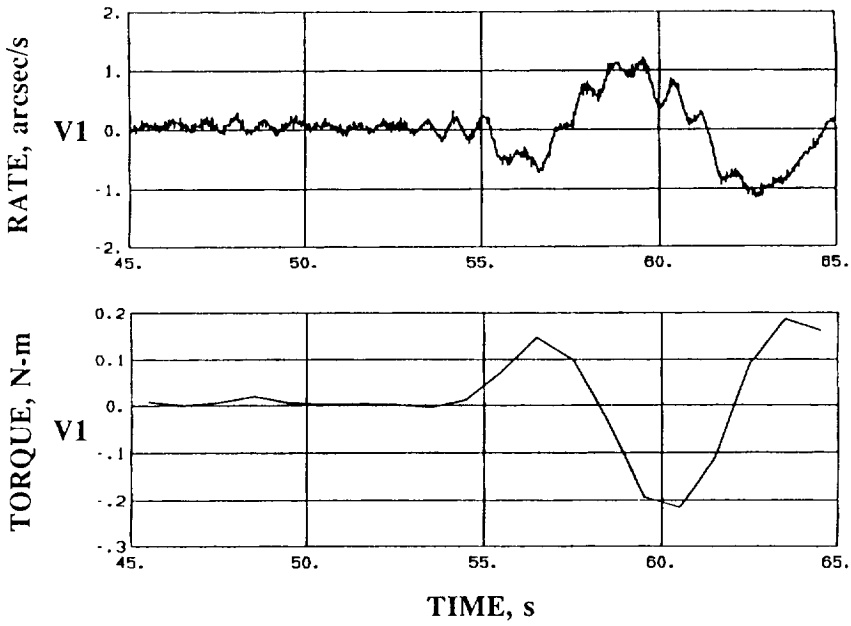

Fig. 13 Comparison of vehicle rates and control torques for V1 axis.

booms (Fig. 2) governed the array deflections due to temperature gradients. Modeling of the booms and calculation of the thermal gradient across them for an eclipse–sunlight transition are described in the next subsection.

Thermal Analysis of Solar-Array Booms

The BI-STEM booms have low mass and in the original arrays experienced considerable thermal excursions. To assess the deflections of the booms induced by thermal gradients, analyses were performed to determine their temperature response. During the course of an orbit, the booms were subjected to time-varying heat rates due to changes in vehicle position and the transitions to and from orbital eclipse. These eclipse transitions contributed the largest variation in heat rates and were of particular interest. Further, the vehicle's inertial orientation, with one side of the booms always oriented toward the sun, inherently caused orbital heating to be concentrated on that side.

As stated in the description of the solar array mechanisms, each array wing has four booms, two per blanket. When each wing was deployed, the booms for one blanket had seams oriented toward the sun while the booms for the other blanket had seams oriented away from the sun. Parametric studies[8] showed that the worst-case heating occurred with the seams oriented away from the sum. To determine the temperature response of the booms, a finite-difference model of a boom cross section was developed as described in Ref. 9. The inner and outer elements, or sleeves, were each represented by 11 nodes, with each node corresponding to 30 deg of arc. A cross section of the boom is shown in Fig. 15 with the radiative surface properties

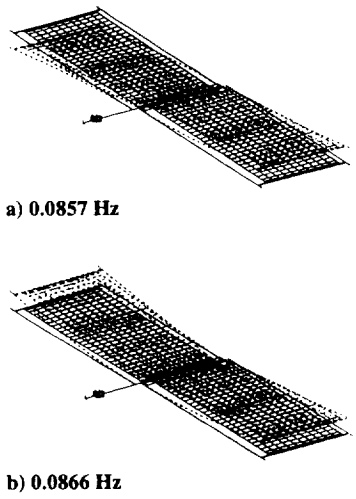

a) 0.0857 Hz

b) 0.0866 Hz

Fig. 14 Fundamental analytical bending modes of solar arrays.

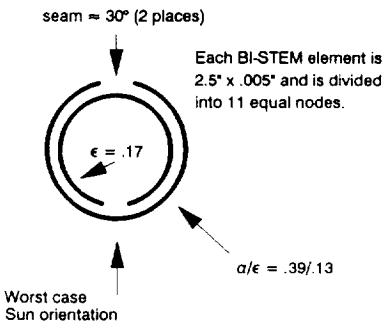

Fig. 15 Solar-array boom cross-section and radiative surface properties.

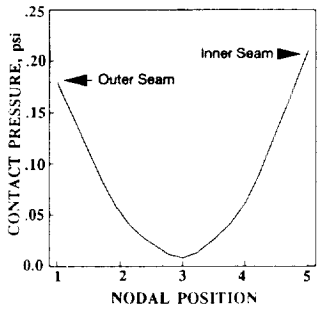

Fig. 16 Contact pressure variation with circumferential position.

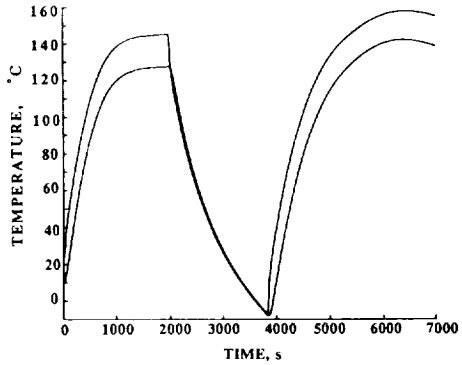

Fig. 17 Predicted temperature profile for solar-array booms.

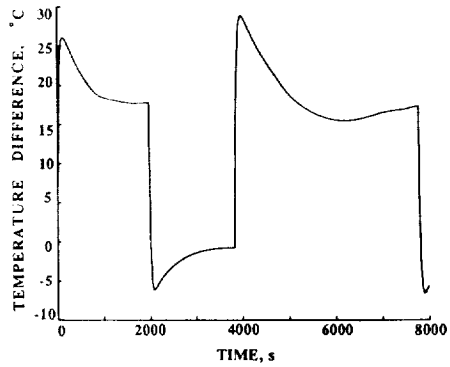

Fig. 18 Analytical orbital temperature gradient for booms.

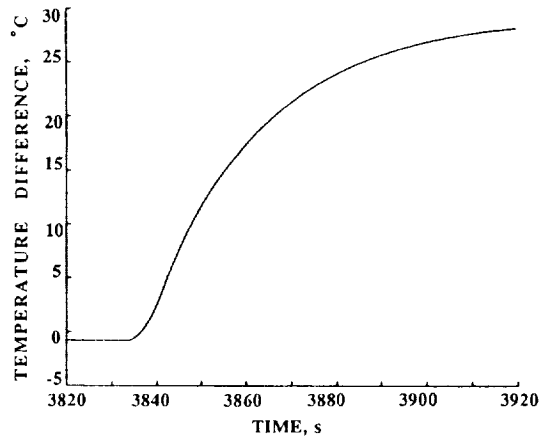

Fig. 19 Boom temperature gradient for eclipse–sunlight transition.

used. Heat rates were calculated based on a 330-n mile orbit, 0-deg beta angle, and nominal flux values. The model incorporated both temperature-dependent thermal conductivity and capacitance. Analyses showed the gradient in the booms to be strongly dependent on the heat-transfer coefficients assumed between the inner and outer sleeves. Since these coefficients are dependent upon contact pressure between the sleeves, estimated contact pressures were factored into the model. Figure 16 shows the estimated contact pressure between the sleeves as a function of circumferential position. The average pressure, 0.074 psi, was equated to a heat-transfer coefficient of 2.5 Btu/h · ft^2 · °F. The specific coefficients were then varied in proportion to the pressure, with the linear equivalent radiation coupling as a lower bound.[9]

In thermal analyses of low-Earth-orbit spacecraft, the solar heat rates are often treated as step functions at the terminators. In actuality, the penumbra moderates the solar influence during the eclipse transitions. With the previously described orbit parameters, the telescope encounters an approximately 17-s penumbra (8.5 s both entering and leaving the eclipse). For these analyses, the penumbra effect was incorporated into the model by linearly ramping the solar heating over the 8.5-s periods. The 0-deg beta angle gave the shortest penumbra period and consequently produced the worst case in terms of how rapidly the gradient is established.

The resulting temperature profile from the analysis for the hottest and coolest areas of the boom cross section is shown in Fig. 17. These areas corresponded to those directly facing the solar flux and to the portion of the inner sleeve exposed by the seam in the outer sleeve, respectively. The temperature gradient, regarded here as the difference in these temperature extremes, is shown in Fig. 18. The orbital position where the vehicle was just entering the sun produced the largest gradient, near 30°C, and a more detailed profile is shown in Fig. 19. This detailed view shows that a 20°C gradient was established quickly, after only 30 s of exposure to the sun. In addition, it is observed that the gradient approximated a quarter sine function. The rate at which the gradient was changing was dynamically more significant (Fig. 20). It is noted that Figs. 15–20 were reproduced from Ref. 9.

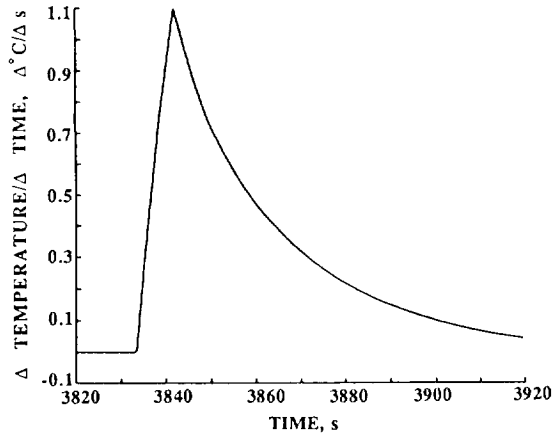

Fig. 20 Rate of change of temperature gradient for booms.

Mechanisms of the Solar-Array Disturbances

In order to identify possible solar-array mechanisms causing the telescope oscillations, the original array geometry was studied in detail. Several geometry characteristics are important to understanding potential sources of vibration. As stated previously, the metal booms used to deploy and support the array blankets governed the thermally induced deflections. These booms have seams that were oriented toward the sun for two arrays and away from the sun for the other arrays. Therefore, the thermal gradients were greater for the arrays with boom seams oriented away from the sun, and the arrays had unequal and probably out-of-phase deflections. Early in the investigation it was thought that these unequal deflections could have caused the observed oscillations; however, continued study showed that this is unlikely.

Another geometry feature of importance is the offset between the booms and the base of each blanket as shown in Fig. 2. Because of this offset and the tension in the blankets, two arrays were pulled toward the sun and the other arrays were pulled away from the sun. It was thought that the thermal stresses induced during orbital transitions could have caused sudden crossover, or snap-through, of the arrays and thus could have initiated the vehicle oscillations. However, previous analysis[10,11] showed that a sudden snap-through of the arrays could not have occurred, but that a smooth crossover or change of curvature was possible. The gradual nature of this crossover precluded the possibility of it causing the disturbances.

Two mechanisms that were considered most likely to cause the vehicle disturbances, especially the orbital day oscillations, were the solar-array drums and spreader bars. The drums are located at the bases of the array blankets (Fig. 2), and in the original design released or retracted the arrays to maintain constant blanket tension during thermal expansion or contraction. According to the European Space Agency, stick–slip effects in the drums due to dry friction could have created high-frequency in-plane blanket modes reacting against the telescope through an interactive torque. This torque could have triggered the 0.1-Hz bending modes of the arrays. The spreader bars are located at the ends of the arrays, as shown in Figs. 2 and 5 for the original design. These mechanisms were originally designed to maintain uniform tension across the blankets, and to move only when something occurred to upset the uniform stress distribution. Soon after release of the telescope from the remote manipulator system, differential bending or twisting of the upper blanket on the −V2 array was observed (Fig. 6). It is possible that this twisting could have caused the spreader bar to experience stick–slip motion on the compensator rails (Fig. 5) and thus to initiate the disturbances, particularly during the orbital day. The deployment sequence anomalies described previously provided additional evidence that the −V2 array was the source of the orbital day disturbances.

In addition to investigating unusual mechanisms or off-nominal behavior as possible causes of the oscillations, it was also considered whether nominal buildup of thermal gradients during transitions could have initiated vibration. Early studies predicted a slow buildup of the thermal gradients, occurring over a period of 300 s, such that significant dynamic effects could not be observed. However, the analysis described in the previous subsection (Fig. 19) showed that the primary portion of the buildup occurred in 50 to 60 s, quickly enough to excite the solar-array bending modes. Further, a static analysis of nominal thermal gradients in the solar arrays showed that torques consistent with telemetry data could be induced on the vehicle by application of a 10-in. tip deflection. Such a tip deflection could be caused by the thermal gradients that occurred across the array booms. Detailed dynamic analyses of the transition disturbances were also performed, and the results compared with telemetry data. Modeling of those events is described in the following subsection.

In summary of the mechanisms discussed in this section, consensus was developed among the investigators that the transitional disturbances most likely arose from nominal thermal gradients in the solar arrays, and that the orbital day disturbances probably arose from stick–slip behavior of the spreader bars or drums. Comparison of the orbital day telemetry data and results of solar-array ground tests provided further evidence that both the spreader bars and the drums were possible sources of the orbital day oscillations. Drum or spreader-bar stick–slip behavior during the orbital day is also thought to have had a residual effect on the night disturbances.

Analytical Modeling of Transitional Disturbances

Although it was realized that analytical models could not prove or disprove the theories concerning the origin of the orbital day disturbances, it was also recognized that analysis could verify or disprove the theorized source of transitional disturbances. In this subsection, open-loop dynamic analyses of the nominal thermal gradient buildup during an eclipse–sunlight transition and the resulting motion of the space telescope are described.

Using the Craig–Bampton method,[12] the equations of motion for the +V2 and −V2 solar arrays were written in reduced form:

$$[M_{sa}]\begin{Bmatrix}\ddot{x}_b\\ \ddot{q}\end{Bmatrix}_{sa}+[K_{sa}]\begin{Bmatrix}x_b\\ q\end{Bmatrix}_{sa}=[\Phi_{sa}]^T\begin{Bmatrix}F_b\\ F_q\end{Bmatrix}_{sa} \tag{1}$$

and coupled with the equations of motion for a rigid telescope body:

$$[M_{c.g.}]\{\ddot{x}_{c.g.}\}=\{F_{c.g.}\} \tag{2}$$

The subscript b indicates forces, accelerations, and displacements corresponding to physical boundary degrees of freedom, and the subscript q corresponds to generalized degrees of freedom. In Eq. (1), $[\Phi_{sa}]$ represents the solar-array mode-shape matrix. The open-loop coupled dynamic equations were written in the form

$$[M_{sys}]\begin{Bmatrix}\ddot{x}_{c.g.}\\ \ddot{q}\end{Bmatrix}_{sys}+[K_{sys}]\begin{Bmatrix}x_{c.g.}\\ q\end{Bmatrix}_{sys}=[\Phi_{sys}]^T\begin{Bmatrix}F_{c.g.}\\ F_q\end{Bmatrix}_{sys} \tag{3}$$

which allows calculation of the telescope c.g. response due to forces applied to the solar arrays. In this formulation, the system modal matrix is given by

$$[\Phi_{sys}]=\begin{bmatrix}\Phi_{c.g.}\\ ---\\ \Phi_{sa}\end{bmatrix} \tag{4}$$

where

$$[\Phi_{c.g.}]=[T_1][\Phi^*_{sys}] \tag{5}$$

$$[\Phi_{sa}]=[\Phi^*_{sa}][T_2][\Phi^*_{sys}] \tag{6}$$

The transformation matrices in Eqs. (5) and (6) are defined in the expressions for the component displacements in terms of the coupled system displacements:

$$\{x_{c.g.}\}=[T_1]\begin{Bmatrix}x_{c.g.}\\ q\end{Bmatrix}_{sys} \tag{7}$$

$$\begin{Bmatrix}x_{c.g.}\\ q\end{Bmatrix}_{sa}=[T_2]\begin{Bmatrix}x_{c.g.}\\ q\end{Bmatrix}_{sys} \tag{8}$$

and the modal matrix $[\Phi^*_{sys}]$ comes from an eigenvalue solution of the free–free coupled equations of motion. Finally, the modified modal matrix $[\Phi^*_{sa}]$ in Eq. (6) is given by

$$[\Phi^*_{sa}] = [R_{sa}]^T [\Phi_{sa}]^T \left([R_{sa}]^T\right)^{-1} \tag{9}$$

where the matrix $[R_{sa}]$ defines the rigid-body transformation from the solar-array boundaries to the space telescope c.g.

To simulate the dynamics of an eclipse–sunlight transition, a set of equivalent solar-array tip forces[5] (corresponding to a nominal 28°C thermal gradient) was used in Eq. (3). As shown in Fig. 21, the gradient and the tip forces were assumed to build up over a 60-s period. It is noted that the assumed tip forces are quarter sine functions. Refined thermal analyses discussed in a previous subsection and on-orbit data showed that the actual solar-array time variations of temperature were close to the assumed functions. Using a 10% difference in the first natural frequencies for the +V2 and −V2 arrays, and the equivalent tip forces described in Fig. 21, the rotational rates of the vehicle were calculated using

$$[I]\{\ddot{q}\} + [2\zeta]\{\dot{q}\} + [\omega^2]\{q\} = [\Phi_{sys}]^T F(t) \tag{10}$$

$$\begin{Bmatrix} \dot{x}_{c.g.} \\ \dot{x}_{sa} \end{Bmatrix} = [\Phi_{sys}]\{\dot{q}\} \tag{11}$$

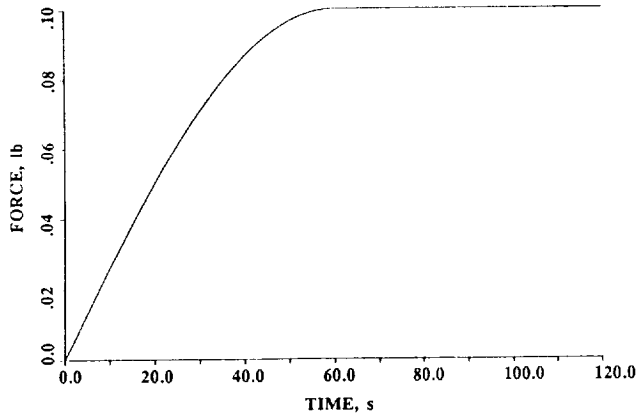

Fig. 21 Solar array tip forces used in modeling of disturbances.

where the mass and stiffness matrices are shown as described in Ref. 12, and ζ is the assumed damping coefficient. The c.g. rotation rates $\{\dot{x}_{c.g.}\}$ are shown in Fig. 22 for the V2 and V3 axes. The response about the V1 axis was approximately two orders of magnitude smaller than about V2 or V3, and smaller than on-orbit V1 disturbances, because of the orientation of the solar-array tip forces along V1. In orbit, the forcing functions likely had significant in-plane components not allowed for in the analysis.

Vehicle rates computed as described in Ref. 5 showed some of the characteristics of the on-orbit data, such as the 0.1-Hz frequency and the beating behavior, and the maximum amplitudes were of the right order of magnitude. Analyses by NASA and European Space Agency investigators for a different array orientation agreed with these results, providing a consensus that the orbital transition disturbances were caused primarily by normal buildup or release of thermal gradients. Although these were open-loop simulations of the transition dynamics, it was previously concluded that the control system could not have initiated the disturbances. Thus the results were conclusive enough to verify the source of transitional disturbances. It is noted that Ref. 13, though not addressing the dynamic interaction of solar arrays and the telescope body, is of interest in view of its detailed treatment of thermally induced vibrations of a cantilever HST solar-array model.

Solutions to the Disturbance Problem

Although the purpose of this paper is to describe the characteristics and the sources of the HST disturbances, a brief discussion of solutions to the problem is presented for completeness. With the determination that the disturbances of the pointing control system were caused by solar-array dynamics, including normal boom vibration due to thermal gradients as well as possible stick–slip behavior of the drums and spreader bars, an extensive two-year effort was undertaken to modify the controller to attenuate the disturbances to tolerable levels. In addition, redesign of the solar arrays was initiated in an attempt to eliminate the source of disturbances.

Control-System Modifications

The first approach considered was to redesign the controller through flight software modifications that could be uplinked to the HST on orbit. Chronological development of these control-law changes is described in detail in Ref. 14. The design approach consisted of three phases: 1) initially implement a compensator to attenuate the 0.1-Hz solar-array out-of-plane bending disturbances,

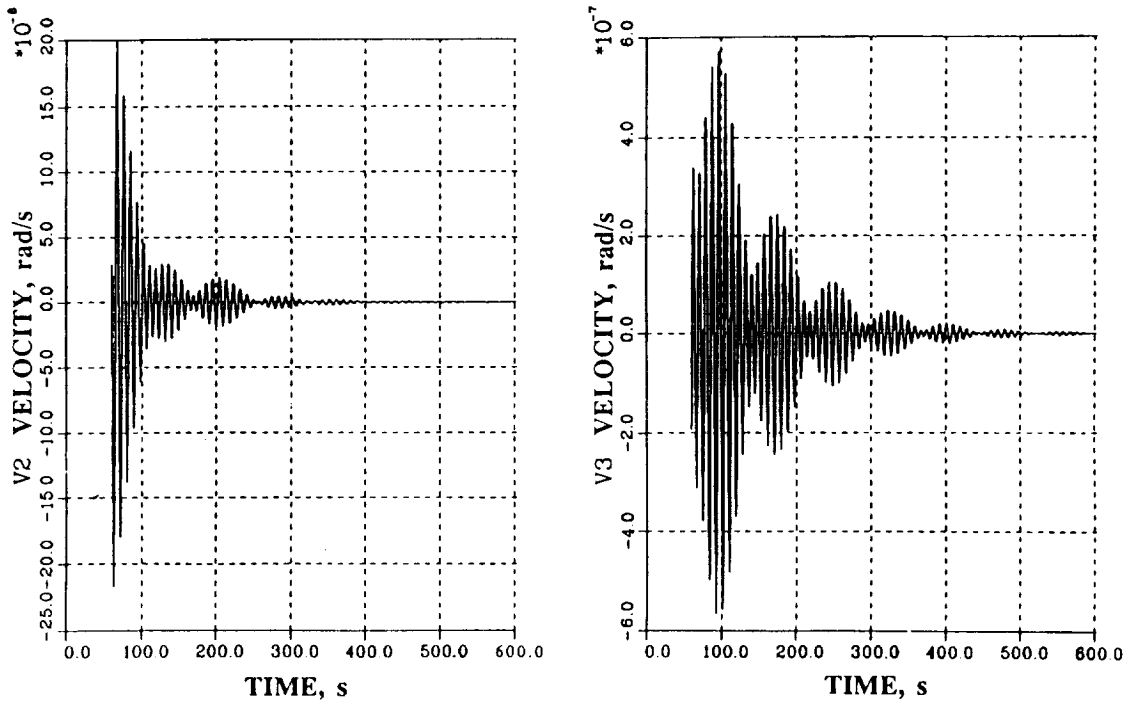

Fig. 22 Response of telescope center of gravity due to solar array tip forces.

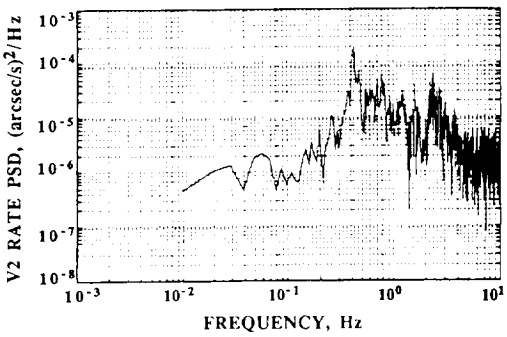

Fig. 23 Frequency response about V2 axis for initial modified controller.

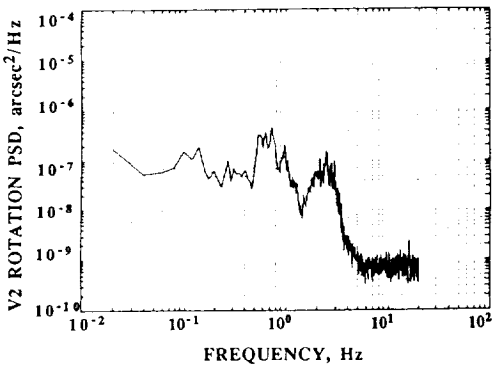

Fig. 24 Response about V2 for second modified controller.

2) perform an on-orbit transfer-function test to help provide an accurate dynamic model of telescope flexible body dynamics, and 3) implement a final compensator to attenuate the remaining disturbances, particularly those due to 0.6-Hz solar array in-plane modes.

Phases 1 and 3 were fully implemented, but an on-orbit transfer-function test was only partially completed.[15] The limited set of measured transfer functions was useful, however, in design of the final or phase 3 compensator. In addition to the initial compensator, a second phase 1 controller was designed having similar attenuation characteristics but being easier to implement.[14] Based upon the success of the second phase 1 compensator in attenuating the 0.1-Hz disturbance, the final compensator was a design that improved the phase 1 controller to allow attenuation of the 0.6-Hz disturbance.

Flight testing verified the predicted characteristics of the redesigned control system. The initial phase 1 controller virtually eliminated the 0.1-Hz disturbance (Fig. 23), but showed undesirable limit-cycle behavior under some conditions. Testing of the second phase 1 compensator showed improved performance, with excessive line-of-sight jitter occurring only during orbital day–night transitions (terminator crossings). As seen in Fig. 24, the higher-frequency 0.6-Hz disturbance still presented difficulty. Finally, the flight test of the phase 3 or final compensator demonstrated the success of the changes in the pointing control system by reducing the 0.6-Hz disturbance as shown in Fig. 25. Dramatic improvements in line-of-sight jitter problems were achieved, making science operations successful about 95% of the time. It may be concluded that changes in the controller were successful in attenuating disturbances to tolerable levels until modified solar arrays could be installed during the HST refurbishment mission. Redesign of the arrays is briefly discussed in the following subsection.

Solar-Array Redesign

As described in previous sections of this paper, it was determined that orbital transition disturbances likely occurred in response to normal buildup or release of thermal gradients in the BI-STEM booms. Thus, one goal of the redesign effort was to reduce the rate of change of the thermal gradient between BI-STEM elements (Figs. 15 and 20) and thus minimize thermal bending of the booms. The solution approach taken by the European Space Agency was to cover the booms with cylindrical thermal shields that would easily

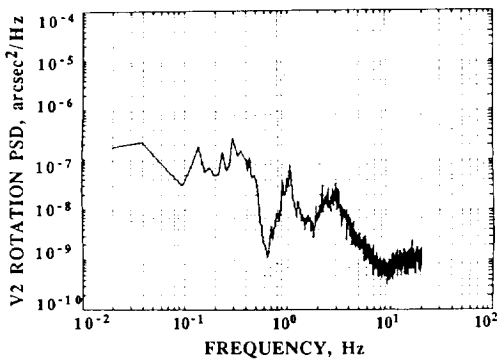

Fig. 25 Frequency response for final modified control system.

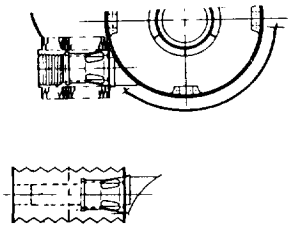

Fig. 26 Thermal shield for redesigned arrays in stowed and deployed configurations.

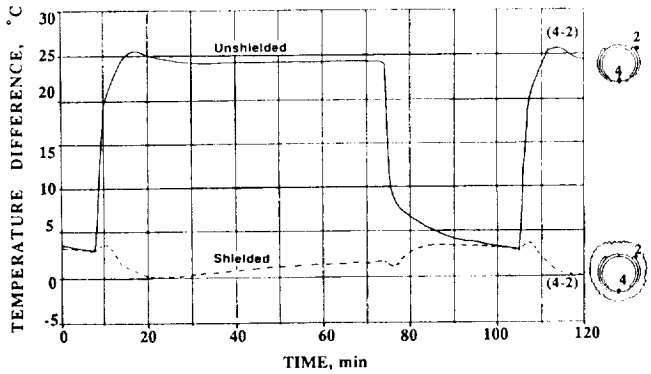

Fig. 27 Reduction in boom thermal gradient due to addition of shields.

deploy and retract with the booms (Fig. 26). A bellows design was utilized with Teflon® outer surface and aluminum inner surface. In Fig. 27, test results show the dramatic reduction in thermal gradient across the BI-STEMs due to addition of the shields.

A second goal of the redesign process was to minimize static and dynamic friction effects in the solar array mechanisms, in view of the consensus of the investigators that orbital day disturbances were likely due to stick–slip behavior of the drums or spreader bars. This goal was accomplished in two steps. First, the boom actuator (Fig. 4) was modified by incorporating a drum brake into the system to prevent drum rotation after array deployment was complete. As discussed earlier in the paper, the drums were originally designed to rotate in response to thermal expansion or contraction of the array blankets and thus maintain constant blanket tension (Fig. 2). Locking the drum with the new brake mechanism required a modification of the blanket tension assembly to provide this compensation. The new tension assembly design, shown in Fig. 28, utilizes 15 soft "bedsprings" attached to the main spreader bar and a new intermediate spreader bar. This new spring system provides the necessary compensation for blanket expansion and contraction without introducing stick–slip frictional effects. Further, the low stiffness of the spring system and the lateral flexibility of the metal bellows at the boom ends compensate for deployment-rate variations between the two booms.

Comparison of Figs. 5 and 28 shows that the original system of steel tapes and rollers has been eliminated, and the potential for stick–slip in the tension mechanism has been reduced. Figure 29 shows a simplified view of an entire redesigned solar array. Initial

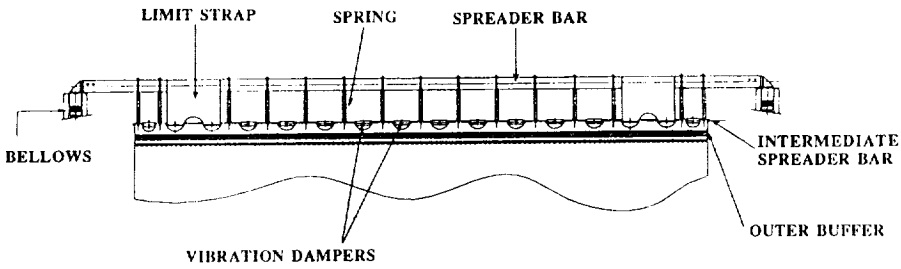

Fig. 28 Redesigned blanket tension assembly for solar arrays.

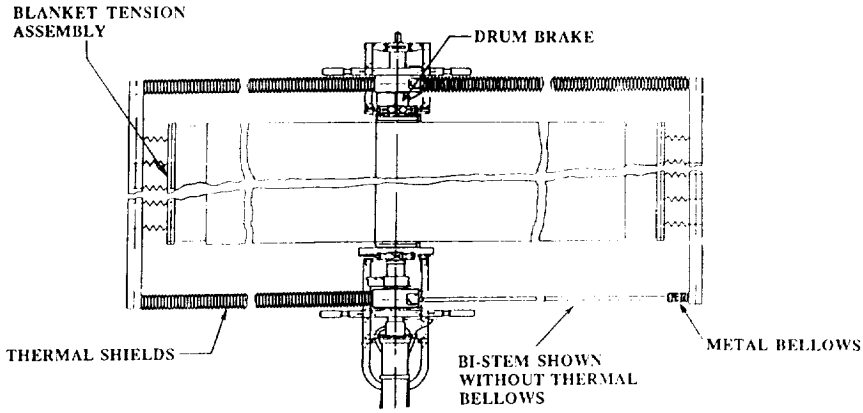

Fig. 29 Simplified overall view of redesigned arrays.

flight data following the HST refurbishment mission in December 1993 indicated that the redesigned solar arrays considerably reduced the disturbances of the pointing control system. The postservicing disturbances without onboard attenuation were comparable to the original disturbances with enhanced control-system attenuation.[16] An on-orbit modal transfer-function test indicated that the modified control algorithm described previously was stable with the new arrays, and the modified controller was activated. The combination of mechanical and thermal changes of the solar arrays and enhanced disturbance attenuation of the control system reduced the pointing-system disturbances to levels below the design requirement of 0.007 arcsec for 95% of the orbit and below 0.012 arcsec for the entire orbit.[16]

Summary

Based on observation of on-orbit telemetry data and results of dynamic mathematical models, it was concluded that orbital transition disturbances of the HST were caused primarily by normal thermal gradients in the solar-array booms. Thermal analyses and on-orbit data showed that the thermal gradients during the early part of eclipse–sunlight transition were similar to quarter sine functions. The orbital day disturbances are thought to have been caused by stick–slip behavior of the solar-array drums or spreader bars. Further, it is thought that the orbital day stick–slip behavior affected the night disturbances.

Control-law modifications were described that reduced the disturbances to levels allowing successful science operations about 95% of the time. The controller redesign was first seen as a temporary measure, pending installation of modified solar arrays during the HST maintenance mission. Redesign of the solar arrays was briefly described, and it was shown that the new arrays have considerably less potential for significant stick–slip behavior and large-amplitude thermal bending that were the sources of disturbances of the pointing control system. Flight data following the refurbishment mission showed that the new solar arrays performed well, and in combination with on-board control-system attenuation minimized the disturbances.

References

[1]Nurre, G. S., and Dougherty, H. J., "The Pointing System for Space Telescope," *The National Symposium and Workshop on Optical Platforms*, edited by C. L. Wyman, Proceedings of SPIE, Vol. 493, Society of Photo-Optical Instrumentation Engineers, Bellingham, WA, June 1984, pp. 2[illegible]–31.

[2]Wolff, G., and Withmann, A., "The Flight of the FRUSA," AIAA Paper 72-510, April 1972.

[3]Cawsey, T. R., "A Deployable Mechanism for the Double Roll-Out Flexible Solar Array on the Space Telescope," *The 16th Aerospace Mechanisms Symposium*, NASA CP-2221, May 1982, pp. 223–233.

[4]Sharkey, J., and Dunker, T., private communication, NASA Marshall Space Flight Center, Huntsville, AL, May 1990.

[5]Blair, M., and Vadlamudi, N., "Hubble Space Telescope Vehicle Rate Anomaly Investigation: Intermediate Results," Lockheed Missiles and Space Co., F373203, Sunnyvale, CA, May 1990.

[6]Hegel, D., private communication, Lockheed Missiles and Space Co., Sunnyvale, CA, May 1990.

[7]Deloo, P., Klein, M., and Reynolds, J., "Solar Array Deployed Finite Element Model: Volume 2," European Space Research and Technology Center, ESA Document TN-SA-0011, Vol. 2, Noordwijk, Netherlands, March 1989.

[8]Kay, S., "Solar Array Bi-stem Thermal Analysis," Lockheed Missiles and Space Co., IDC TCS/01-003, Sunnyvale, CA, May 1990.

[9]Kay, S., and Yoshikawa, Y., "Solar Array Bi-stem Thermal Analyses," Lockheed Missiles and Space Co., EM TCS512, Sunnyvale, CA, Aug. 1990.

[10]Davies, W. V., "Analysis of Bistem Booms to Ascertain Possibility of 'Snap Through' Due to Thermal Gradients," British Aerospace, ESA Document TN-SA-B638, Bristol, England, UK, May 1986.

[11]Klein, M., "Thermal Induced Solar Array Disturbances," European Space Research and Technology Center, ESA Document TN-SA-0001, Noordwijk, Netherlands, Oct. 1985.

[12]Craig, R., and Bampton, M., "Coupling of Substructures for Dynamic Analysis," *AIAA Journal*, Vol. 6, No. 7, 1968, pp. 1313–1319.

[13]Thornton, E. A., and Kim, Y. A., "Thermally Induced Bending Vibrations of a Flexible Rolled-Up Solar Array," *Journal of Spacecraft and Rockets*, Vol. 30, No. 4, 1993, pp. 438–448.

[14]Sharkey, J., Nurre, G., Beals, G., and Nelson, J., "A Chronology of the On-Orbit Pointing Control System Changes on the Hubble Space Telescope and Associated Pointing Improvements," AIAA Paper 92-4618, Aug. 1992.

[15]Vadlamudi, N., Blair, M. A., and Clapp, B. R., "Hubble Space Telescope On-Orbit Transfer Function Test," AIAA Paper 92-4614, Aug. 1992.

[16]Anderson, G., Bradley, A., Kelley, J., Nelson, J., and Dougherty, H., "HST Pre-Servicing Mission Overview and Servicing Mission Results," *The 13th International Federation of Automatic Control Symposium on Automatic Control in Aerospace*, Pergamon, Oxford, England, UK, 1994.

E. A. Thornton
Associate Editor